Insight into Dehydrogenation of C_2H_X Species in Ethane Steam Reforming on Ir(100): A DFT Study

Rotimi M. Ore, Ruitao Wu, and Lichang Wang*

School of Chemical and Biomolecular Sciences and the Materials Technology Center, Southern Illinois University, Carbondale, Illinois 62901, USA

ABSTRACT

The reaction barrier and heat of formation of various dehydrogenation reactions involved in the steam reforming of ethane (SRE) are critical parameters in the understanding and improving the technology of SRE. Focusing on Ir-based catalyst, we report a comprehensive reaction network of dehydrogenation of ethane on Ir(100) based on extensive density functional theory (DFT) calculations on 10 C-H bond cleavage reactions. The geometric and electronic structures of the adsorption of C_2H_x species with corresponding transition-state and product structures are reported. We found that the C-H bond in CH_3C required the most energy to activate, due to the most stable four-fold hollow configuration of the adsorption site. Ethane can easily dissociate to CH_3CH and CH_2CH_2 on Ir(100). By using the degree of dehydrogenation of the reactant species as a variable to correlate the C-H bond cleavage barrier as well as reaction energy, DFT results reveal that the Ir(100) surface to a great extent promotes ethane dehydrogenation when compared to other surfaces.

*Correspondence author: lwang@chem.siu.edu.

1. INTRODUCTION

Due to increasing demand for light alkenes and their products, the conversion of starting materials such as light alkanes,[1-11] alcohols,[12-16] carbon dioxide,[17-23] has become an important industrial process. Steam cracking of natural gas[16, 24-31] and naphtha[32-34] as well as fluid catalytic cracking in oil refining has been among the earliest techniques employed. Recent efforts have focused on developing less energy intensive and more selective alternatives to steam cracking. The catalytic dehydrogenation[7, 35-46] and oxidative dehydrogenation[47-57] of C_{2+} light alkanes to olefins is of industrial interest. C-H sigma bond activation in light alkanes plays an important role in its transformation to value-added chemicals for other technological applications.[58-67] The major challenge facing the catalytic dehydrogenation of alkanes is the inert nature of C-H sigma bond at low temperatures and the ubiquitous coke deposition at high temperatures. To mitigate these challenges, H_2, H_2O(g) and CO_2 have been frequently employed as auxiliary reactants during the dehydrogenation process. However, the use of H_2 as an auxiliary gas will decrease the equilibrium conversion of dehydrogenation, the presence of CO_2 could result in H_2O(g) formation. Hence, effective dehydrogenation of ethane and other light alkenes is actively being studied both experimentally and theoretically, with considerable attention to the utilization of transition metals to catalyze C-H bond activation in alkanes.

Several papers have reported on metal based catalysts[39, 43] and metal oxide based catalysts.[39, 68] The effect of promoters such as Zr[69] and Zn,[70] surface elements such as phosphorus,[56] tin[71] as well as high temperature pretreatment[72] have been reported. The role of carbon dioxide[57, 68-69, 73-75] has been shown to assist in the dehydrogenation process. Our interest however lies in the dehyrogenation of ethane[39, 41, 48, 53-54, 68-69, 73-74, 76-84] and specifically dealing with Ir-based[83, 85] catalysts although reports show other suitable metal based ethane dehydrogenation catalysts, such

as Co,[72, 75, 83] Cr,[57, 69, 73, 86] Fe,[87] Ga,[74, 82, 88-89] Ni,[83, 90] Pd,[77, 83, 91-92] Pt,[70, 78-81, 83, 93-94] V[95] as well as metal alloys Fe-Ni,[90] Pd-In,[77] Pd-Ir,[96] Pt-Ir,[78] and Metal-Phosphides.[84, 97] Transition metal clusters, especially platinum (Pt) reduce the energy barrier both in gas phase and on a metal oxide surface thereby leading to C-H bonds cleavage at lower temperatures. However, loss of catalytic activity has been observed as clusters, such as Pt clusters, coalesce very easily in the gas phase and much more difficultly at higher reaction temperatures when supported by a metal oxide surface. Pt catalysts are well known to be very active but with poor selectivity and rapid catalyst deactivation. Ir-based catalysts are promising when compared to inabundant Pt or toxic Cr catalysts that suffer from thermodynamically promoted coke formation.

Iridium (Ir) clusters have been studied widely[98-100] and also shown tremendous potential toward activating the C-H bonds of ethane in gas phase and on metal oxide surfaces. Ethane dehydrogenation on $IrO_2(110)$,[101] shows that ethane forms strongly bound σ-complexes on $IrO_2(110)$ and can undergo C−H bond cleavage at temperatures below 200 K. It was also seen that a large portion of the dehydrogenation was purely because of heating, and partially hydrogenating the surface enhanced the dehydrogenation. There exists a trade-off between improved catalytic activity and cluster size,[102-103] studies show that small transition metal clusters migrate easily on the metal oxide surface. Hence, while enhancing the catalytic ability of the transition metal clusters, migration, coalescence, and deactivation should be prevented.[104] The dependence of catalytic activity of Ir clusters on cluster size and catalytic sites has been studied.[105]

This work aims to report the studies of ethane dehydrogenation on Ir(100) to provide insight on the reaction network of ethane dehydrogenation, and ultimately to the improvement of the dehydrogenation of ethane to value added products. Density function theory (DFT) studies reveal that the surface Ir(100) to a great extent promotes ethane dehydrogenation when compared to other

surfaces. Results demonstrated that ethane dehydrogenation on Ir(100) resulted in a low energy barrier of the C−H bond activation, this we speculated is primarily due to the Ir(100) surface.

2. COMPUTATIONAL DETAILS

DFT calculations utilizing the Vienna Ab-initio Simulation Package (VASP)[106-107] were performed to study ten elementary ethane dehydrogenation reactions. The Perdew-Burke-Ernzerhof (PBE) functional was used to describe the exchange-correlation interactions. To describe effective core potentials, i.e., the interaction between the core and valence electrons, Projector Augmented Wave (PAW) method[108-109] was used. All investigations in this work were carried out on a periodic (4x4) slab with four Ir layers of (100) facet, built from the Ir-bulk with lattice constant of 3.875Å. Computationally reported lattice constant 3.882Å and 3.877Å[21] agree well. Interactions between adsorbates and their horizontal periodic images were eliminated by a 10Å spacing. To prevent artificial interactions between the slab surface and its periodic image, a 15Å vertical vacuum space was placed between such images. The model catalyst is shown in Figure 1. In this work three main calculations performed were geometry optimization, transition state search, and frequency calculations.

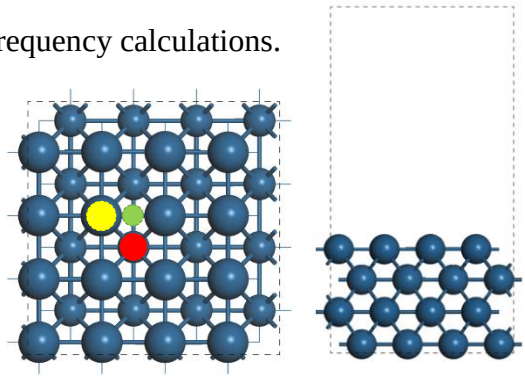

FIG. 1. Top view (left) and side view (right) of Ir(100). Yellow, red, and green circles represent atop, bridge and hollow sites respectively. The Ir atoms on the second layer of top view were made smaller in size to differentiate them from the Ir atoms on the first layer.

The bottom two layers were fixed during optimization and transition state calculations, while the top two layers were allowed to relax. Only the atoms in the top layer were allowed to relax in frequency calculations. This same model of catalyst was used in our previous works.[46, 110-112] A cutoff energy of 400eV was set in the plane wave basis set. The Brillouin zone was sampled using a 2x2x1 K-point grid. Convergence was achieved in optimization calculations when the Hellmann-Feynman forces was less than 0.02eV/Å. The optimized structures of reactants and products were further verified by frequency calculations yielding no imaginary frequency. The transition states were obtained using the Climbing Nudged Elastic Band (CI-NEB) method[113] and verified with the presence of one imaginary frequency. The optimized structures of all studied reactions are presented in section 3. For non-transition state structures possessing one imaginary frequency significantly less than 100cm^{-1}, negligible effect on the total energy less than 0.05eV was observed once that the imaginary frequency is removed as shown in Table 1.

Table 1. The energy and structural parameters of ethane with and without an imaginary frequency.

	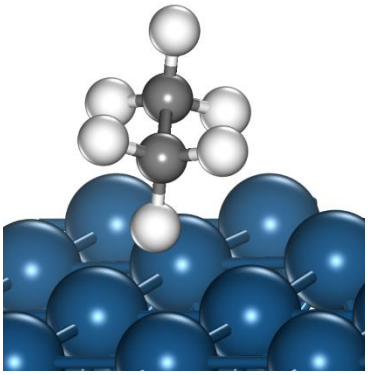	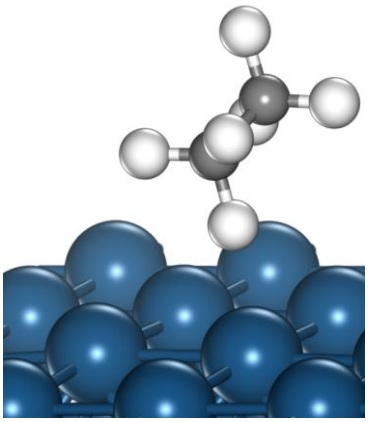
C-H Length (Å)	1.140	1.133
Total Energy (eV)	-561.8086	-561.8085
Imaginary Frequency (cm^{-1})	41.4	---
Zero Point Energy (eV)	2.3219	2.3214

The activation energy (E_a) and reaction energy (ΔE) of the studied reactions was calculated according to the equations

$$E_a = E_{TS/slab} - E_{IS/slab} \quad (1)$$

$$\Delta E = E_{FS/slab} - E_{IS/slab} \quad (2)$$

where $E_{IS/slab}$, $E_{TS/slab,}$ and $E_{FS/slab}$ are the zero-point energy (ZPE) corrected total energies of an adsorbed species on the Ir(100) surface for the initial state (IS), transition state (TS), and final state (FS), respectively. All calculated energies reported have been Zero-Point-Energy (ZPE) corrected using

$$E_{ZPE} = \sum_{i=1}^{k} \frac{hv_i}{2} \quad (3)$$

where h and v_i denote the Planck's constant and vibrational frequencies. Further investigation of the electronic structure and distribution of electrons in adsorbates were carried out by Density of States (DOS) and Bader Charge analysis.[114] The net charge was calculated by subtracting the Bader charge from the original outmost electron number of each element. A negative and positive net charge represents electron gain and loss, respectively.

3. RESULTS AND DISCUSSION

This work investigated the C-H bond cleavages of ethane and the various intermediates, over Ir(100). Extensive DFT calculations were used to obtain the reaction network providing insight to the geometries and energetics of the initial states (ISs), transition states (TSs), and final states (FSs). From optimized structural results it is evident that on Ir(100) the CH_x fragment preferentially adsorbs to possess tetravalency. As such, CH_3 is not bound to the surface, while CH_2

is adsorbed on the atop site, CH is adsorbed on the bridge site except when bound to CH_2, and C adsorbs on the bridge site except when bound to CH_2. It is seen that in other for CH_2 to keep its preferentially adsorbed site, CH_2 causes CH and C to be adsorbed on the atop and hollow site respectively.

Table 2 summarizes the values for activation and reaction energies with correlation to the degree of dehydrogenation, energy values account for ZPE correction. C-H bonds are not easily broken and based on the DFT results achieved, the reactions that have an activation energy of more than ~0.72 eV[110] would generally not proceed under room temperature, and as such we speculate that the dehydrogenation of CH_3C and CHC are the most difficult steps. The difficulty to cleave the C-H bond increases with increase in activation energy, which is suspected to have a dependence on the degree of dehydrogenation. This suggests that at room temperature, the dehydrogenation of species with DoDH less than 50% is relatively less involved than that with DoDH more than 50% except for CH_2C specie. In what follows, we will first present the results of the elementary reactions with degree of dehydrogenation of less than 50% in Section 3.1, followed by those of degree of dehydrogenation of 50% and above in Section 3.2. The role of O and OH species on the activation of C-H bond in ethane is discussed in Section 3.3 and our results are compared and correlated with previously studied reactions for C-C bond cleavage in SER on Ir(100)[111] and data from C_XH_Y-O species in EOR on Ir(100).[46, 110, 112] The discussion of results concludes with a descriptive insight to the reaction configuration space and activation energy surfaces.

Table 2. The activation barrier (Ea) and reaction energy (ΔE) of 12 C–H bond cleavage reactions on Ir(100).

Label	Reaction	DoDH	E_a	ΔE
	-H	%	eV	eV
1	CH_3CH_3 → CH_3CH_2	0	0.09	-0.64
2	CH_3CH_2 → CH_3CH	16.7	0.04	-0.53
3	CH_3CH_2 → CH_2CH_2	16.7	0.09	-0.42
4	CH_3CH → CH_3C	33.3	0.24	-0.93
5	CH_3CH → CH_2CH	33.3	0.36	-1.20
6	CH_2CH_2 → CH_2CH	33.3	0.20	-1.03
7	CH_2CH → CHCH	50.0	0.28	-1.62
8	CH_2CH → CH_2C	50.0	0.01	-1.06
9	CH_3C → CH_2C	50.0	1.08	-0.27
10	CH_2C → CHC	66.7	0.07*	-0.64*
11	CHCH → CHC	66.7	0.63	-0.09
12	CHC → CC	83.3	1.04*	0.57*

*Data was taken from ref. [46]

3.1 The C-H bond activations in reactive species with DoDH less than 50%.

The 6 reactions investigated herein include reactions **1-6**. The corresponding optimized structures for the initial state (IS), transition state (TS) and final state (FS) are presented in Figure 2 for the first three reactions with the C-H bond distances for various structures summarized in Table 3. The first dehydrogenation of ethane leads to the formation of a CH_3CH_2 specie with C-H cleavage barrier of 0.09eV, is suspected to be the most crucial step leading to CH_2CH_2 specie, with a reaction energy of -0.64eV.

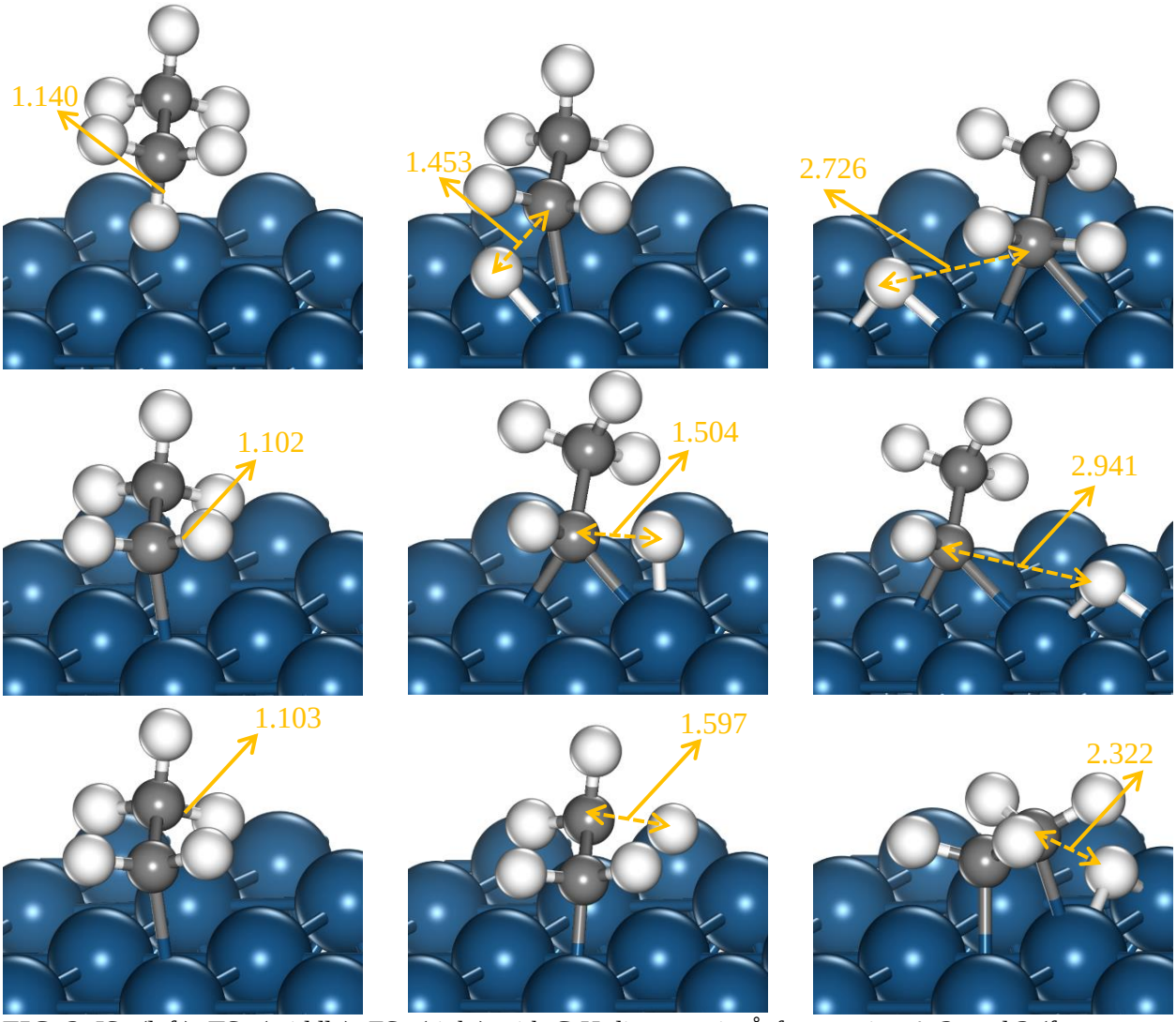

FIG. 2. ISs (left), TSs (middle), FSs (right) with C-H distances in Å for reaction **1**, **2**, and **3** (from top to bottom), respectively.

Although the six H atoms are similar in the C_2H_6 species, it is worth noting that the overlap, relative position, and distance of each H atom from the catalyst surface determines the preferentially dehydrogenated H atom. This is illustrated in the DOS plots of the selected atoms in the initial configuration of ethane in Figure 3.

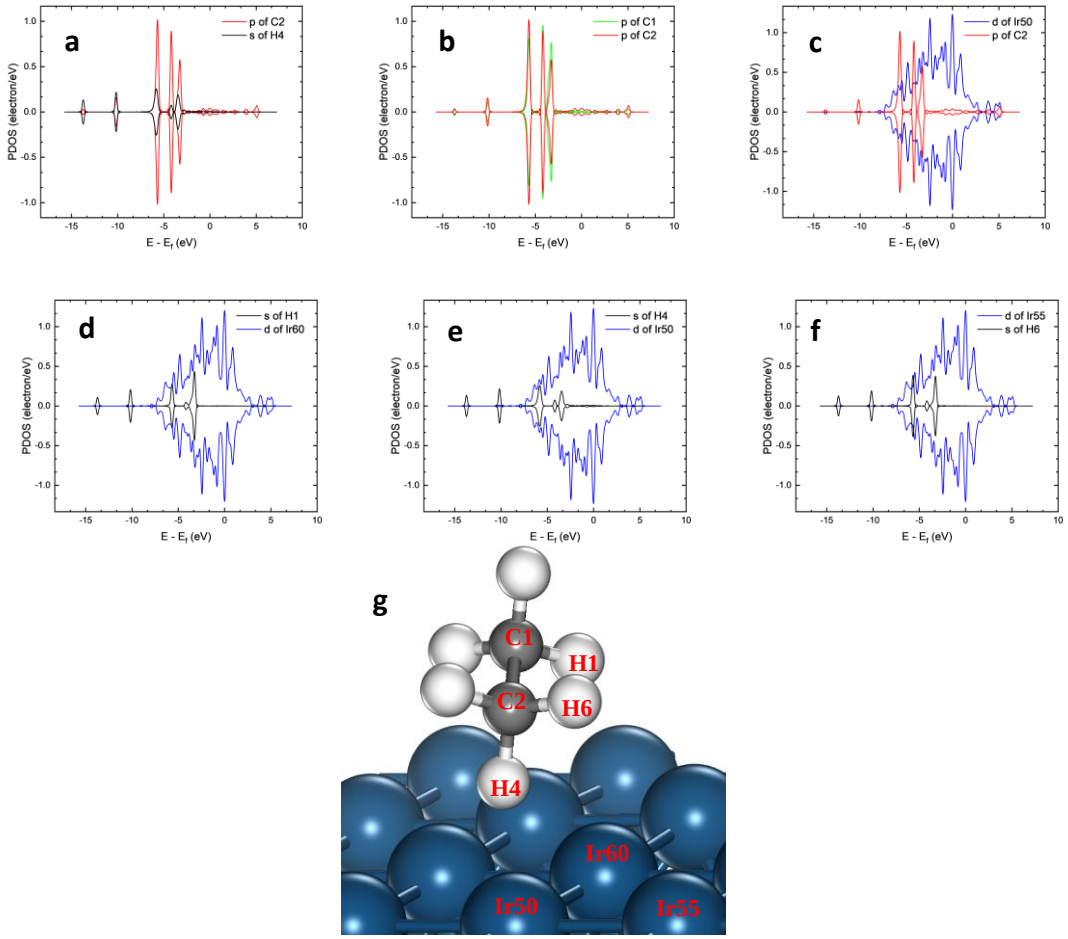

FIG. 3. The s, p-projected DOSs for (a) C2-H4, p, p-projected DOSs for (b) C1-C2, p, d-projected DOSs for (c) C2-Ir50 bonds, and the s, d-projected DOSs for the interactions (d) Ir60 and H1, (e) Ir50 and H4, (f) Ir55 and H6 in the initial configuration of ethane (g). The distances between the labelled H and its nearby Ir are d(H1-Ir60) = 3.318 Å, d(H4-Ir50) = 2.118 Å, and d(H6-Ir55) =3.661 Å.

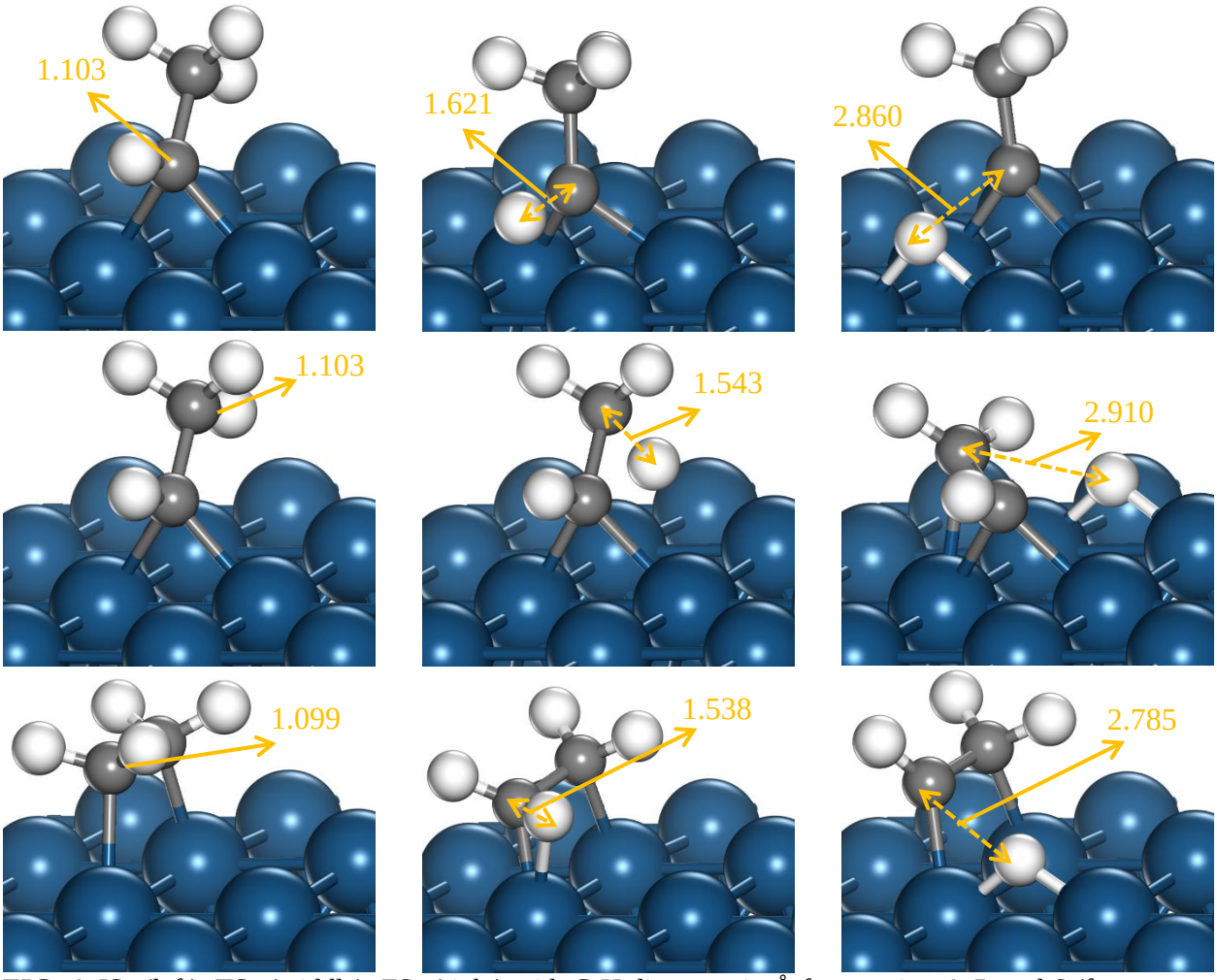

FIG. 4. ISs (left), TSs (middle), FSs (right) with C-H distances in Å for reaction **4**, **5**, and **6** (from top to bottom), respectively.

Hence it is necessary to investigate how the deviation from a fully saturated carbon and loss of symmetry influences the adsorption of the species on Ir(100) surface. There are two types of C atoms in our system, termed C1 and C2, C1 indicates the more highly substituted C atom and C2 is the other C atom. When both C atoms are equally substituted and symmetrical, they are equivalent. From Table 2 dehydrogenation from C1 has a higher barrier than dehydrogenation from C2.

Table 3. C-H Bond distance of species with DoDH less than 50%.

Label	DoDH (%)	C-H Distance (Å)		
		Initial State	**Transition State**	**Final State**
1	0	1.140	1.453	2.726
2	16.7	1.102	1.504	2.941
3	16.7	1.103	1.597	2.322
4	33.3	1.103	1.621	2.860
5	33.3	1.103	1.543	2.910
6	33.3	1.099	1.538	2.785

Although the dehydrogenation from either C1 or C2 in CH_3CH_2 have almost the same activation barrier, the following dehydrogenation of CH_3CH and CH_2CH has a higher activation barrier when the H being cleaved is bound to C1, this trend accounts for the required increase in activation energy to activate the C-H bond in CH_3C. Also, the reaction energy and because it is easier to dehydrogenate from C2 due to lower activation energy, CH_3C is a thermodynamically likely product although CH_3C might poison the catalytic surface.

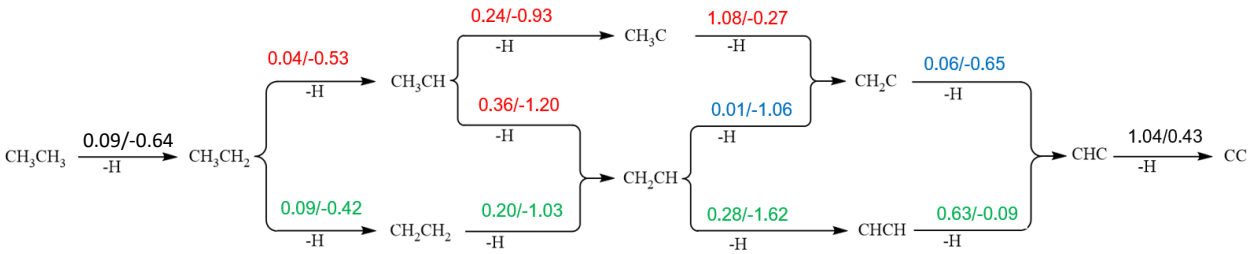

FIG. 5. Calculated reaction network for the ethane dehydrogenation on Ir(100). The energy barriers (left) and reaction energies (right) are shown above the arrows. The numbers are in a unit of eV.

When CH_3CH_2 is dehydrogenated via reaction **2**, the transition state links to three bridge sites that are possible to adsorb the cleaved H, each pathway was investigated, and the minimum energy pathway is reported here with geometry structures shown above. It was observed that the (IS)

diffuses from an atop site to a more stable geometry at the bridge site that is linked by the (TS) to the (FS). The different activation barriers and reaction energy of the various pathways can be seen in Figure 5.

Table 4. E_a of species with DoDH less than 50% compared for Ir(100), Pt(111), and Pt(211).

Label	Reaction	Ir(100)	Pt(111)[115]	Pt(211)[115]
	-H	eV	eV	eV
1	$CH_3CH_3 \rightarrow CH_3CH_2$	0.09	0.54	0.08
2	$CH_3CH_2 \rightarrow CH_3CH$	0.04	0.88	0.27
3	$CH_3CH_2 \rightarrow CH_2CH_2$	0.09	0.81	0.44
4	$CH_3CH \rightarrow CH_3C$	0.24	0.28	0.86
5	$CH_3CH \rightarrow CH_2CH$	0.36	0.71	0.92
6	$CH_2CH_2 \rightarrow CH_2CH$	0.20	0.84	0.57

CH_3CH can be dehydrogenated via reactions **4** and **5**, the reaction barrier and reaction energy for both reactions are 0.24eV/-0.93eV & 0.36eV/-1.2eV. When CH_3CH is dehydrogenated via reaction **4**, further dehydrogenation to CH_2C becomes more difficult. DFT results will be able to give insight on the correlation between degree of dehydrogenation and the activation barrier. As well as to identify the dominant factors for C-H activation out of factors such as the activation degree of C-H bond, and interaction between (TS) and catalyst surface. When correlated with the activation barrier and reaction energy, the greater the C-H bond distance in the (FS) might be an indicator that the C-H bond in (IS) was easier to break. A correlation between the ease of C-H cleavage and the distance from the C-H bond to the catalyst surface will also be possible.

3.2 The C-H bond activations in the species with DoDH of 50% and above.

The six reactions investigated herein include reactions **7-12**. The corresponding optimized structures for the initial state (IS), transition state (TS) and final state (FS) are presented in Figures 6 and 7**.** The C-H bond distances for the various structures are summarized in Table 5**.** CH_2CH can be dehydrogenated via reactions **7** and **8**, with both reactions leading to an adsorbed specie having

50% degree of dehydrogenation. The reaction barrier and reaction energy for both reactions are 0.28eV/-1.62eV & 0.01eV/-1.06eV.

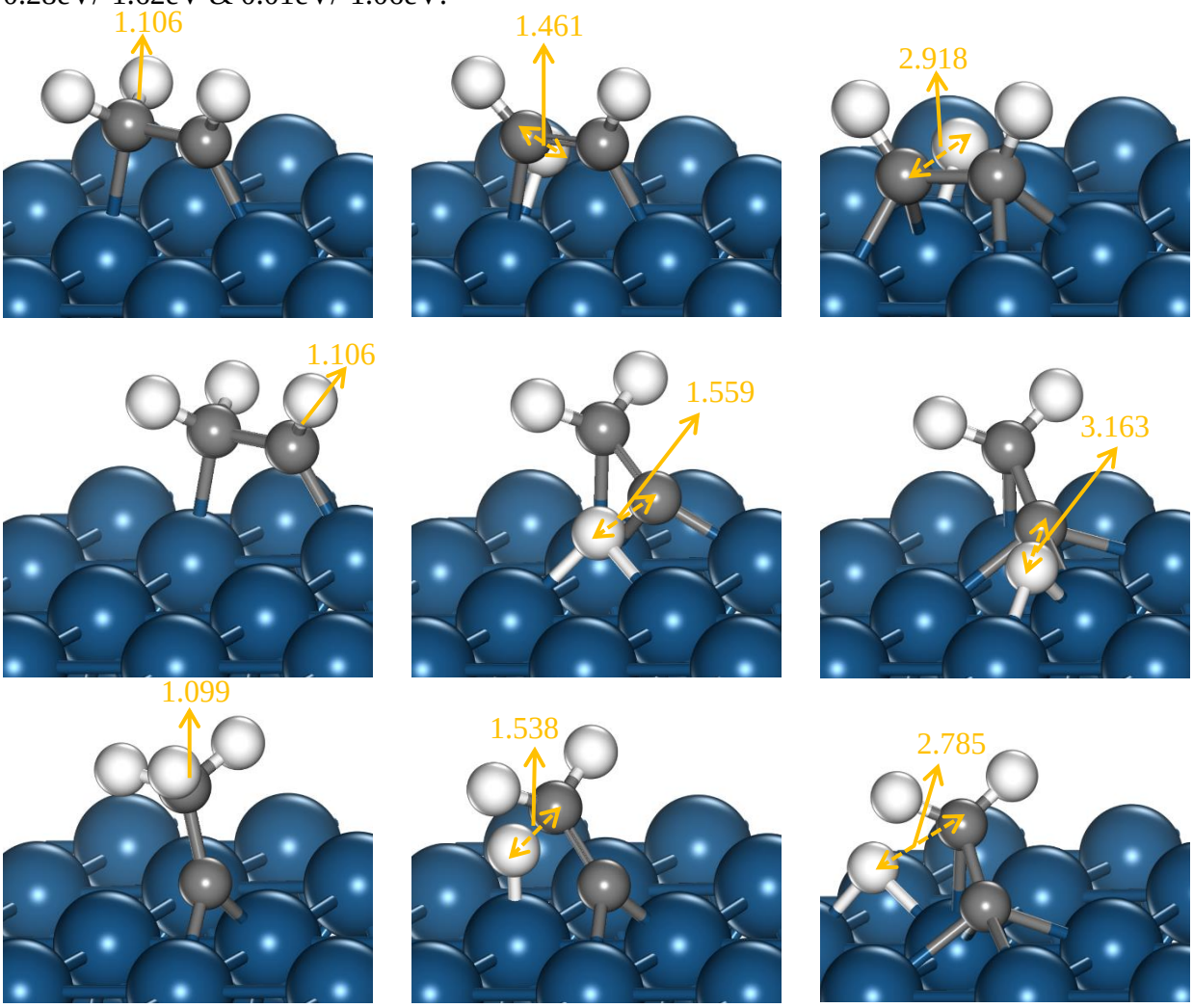

FIG. 6. ISs (left), TSs (middle), FSs (right) with C-H distances in Å for reaction **7, 8,** and **9** (from top to bottom), respectively.

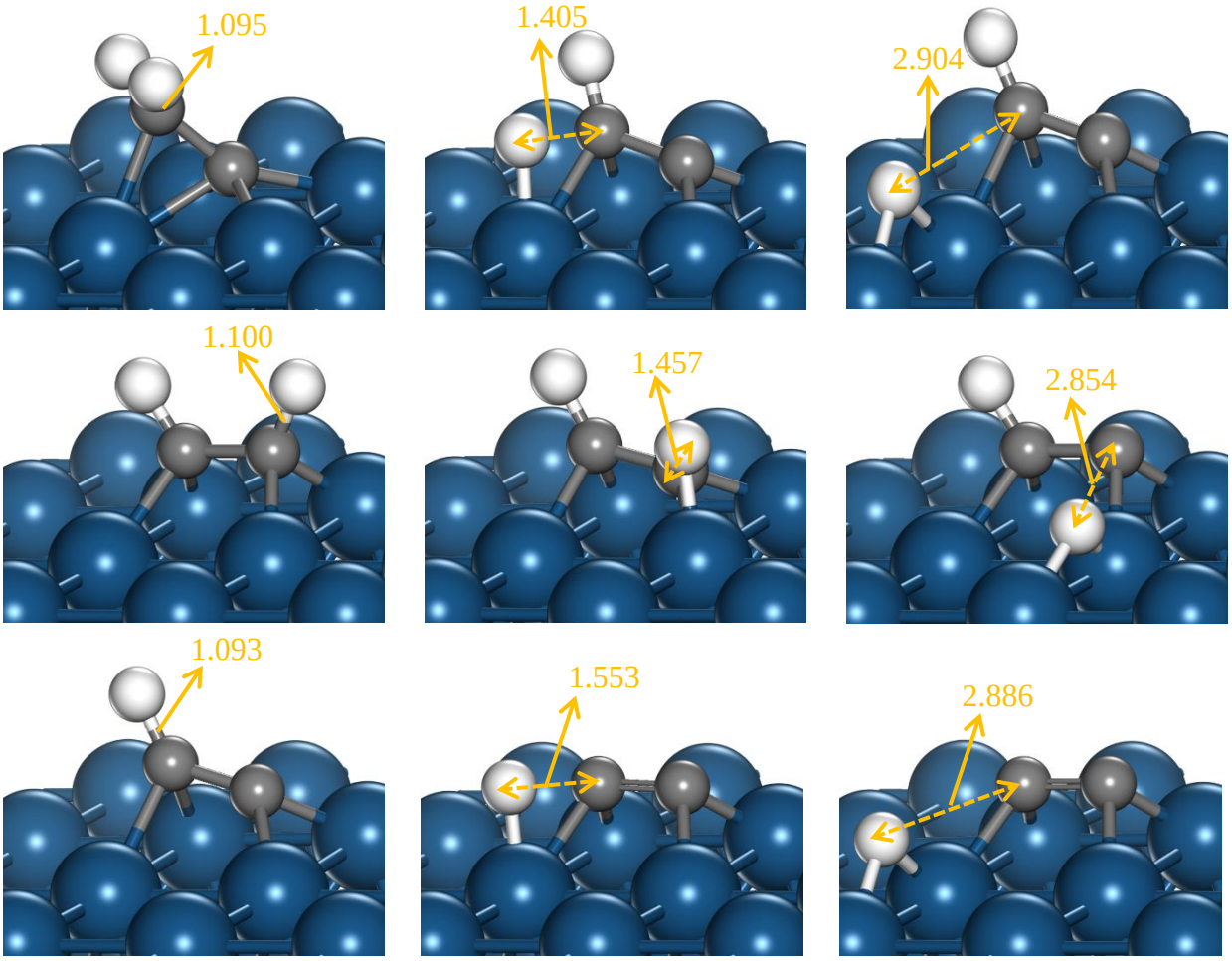

FIG. 7. ISs (left), TSs (middle), FSs (right) with C-H distances in Å for reaction **10**, **11**, and **12** (from top to bottom), respectively.

Table 5. C-H Bond distance of species with DoDH of 50% and above.

Label	DoDH (%)	C-H Distance (Å)		
		Initial State	**Transition State**	**Final State**
7	50.0	1.106	1.461	2.918
8	50.0	1.106	1.559	3.163
9	50.0	1.104	1.726	2.609
10	66.7	1.095	1.405	2.904
11	66.7	1.100	1.457	2.854
12	83.3	1.093	1.553	2.886

The structure of CH_3C we used in the calculations is about 0.29eV less stable than the most stable adsorption geometry for CH_3C reported in Figure 8. Reaction **12**, which is the final dehydrogenation product with degree of dehydrogenation of 100%, shows how CC double bond is absorbed on the catalytic surface. The most stable adsorption geometry of this specie is parallel to the catalytic surface at the hollow site. A trend in the adsorption configuration can be seen in species that are symmetric at both ends of the bond. These species include C-C(100% DoDH), HC-CH(66.7% DoDH), H_2C-CH_2(33% DoDH) and the starting molecule H_3C-CH_3. If this trend is followed, ongoing calculations for the first dehydrogenation step should see similar adsorption geometry. The most stable adsorption site being the hollow site, followed by the bridge site.

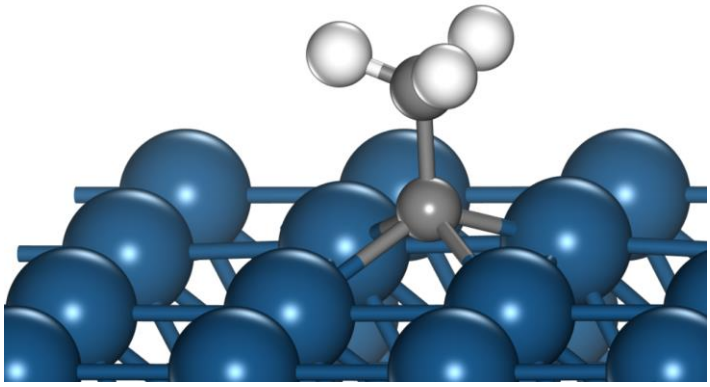

Figure 8. Most stable four-fold hollow adsorption site configuration of CH_3C.

Table 6. E_a of species with DoDH less than 50% compared for Ir(100), Pt(111), and Pt(211).

Label	Reaction	Ir(100)	Pt(111)[115]	Pt(211)[115]
	-H	eV	eV	eV
7	CH_2CH → CHCH	0.28	1.03	1.13
8	CH_2CH → CH_2C	0.01	0.70	0.66
9	CH_3C → CH_2C	1.08	1.33	1.30
10	CH_2C → CHC	0.06*	2.22	1.67
11	CHCH → CHC	0.63	2.12	1.19
12	CHC → CC	1.04*	--	--

*Data was taken from ref. [46].

It is worthwhile to compare the dehydrogenation of ethane to those of methane.[116] It was also found that Ir[117] is easier to activate the C-H bond than Pt[118] and Ni.[119] This suggests that Ir is a good dehydrogenation catalysts regardless of chain length of alkane. Interestingly, Ir is also a good catalyst for water dissociation.[120]

3.3 Activation Energy Surface and Reaction Energy Surface of Dehydrogenation Reactions

In steam reforming of ethane, the O from dissociated water can be presence and affect dehydrogenation of ethane. Therefore, we investigated the Role of O and OH species on the C-H activation in ethane. Species classified as C_2H_XO have previously been reported.[112, 121-122] Unlike C-C bond cleavage in ethane, where the presence of O lowers the C-C bond activation barrier,[123] the results shown in Table 7 indicates that the presence of O increases the dehydrogenation barrier. Although these barriers are still lower than the dehydrogenation on other catalysts, such as Cu.[124-126] The better catalytic ability to dehydrogenate by Ir is the same for C-C bond cleavage with respect to Cu based.[127-130]

Table 7. Activation and reaction energy surface data for C–H bond cleavage reactions on Ir(100).

Reactant	DoDH	DoBC	E_a	ΔE	Reactant	DoDH	DoBC	E_a	ΔE
	%	%	eV	eV		%	%	eV	eV
CH_3CH_3	0	10	0.09	-0.64	$CHCH_2O$	50	50	0.59	0.01
CH_3CH_2OH	0	0	0.3	-0.57	CH_2CHO	50	55	0.24	-0.82
CH_3CH_3	0	10	0.09	-0.64	CH_3CO	50	60	0.42	-0.36
CH_2CH_2OH	16.7	10	0.59	-0.6	CH_2CH	50	65	0.01	-1.06
CH_3CHOH	16.7	15	0.16	-0.64	CH_3C	50	70	1.08	-0.27
CH_3CH_2O	16.7	30	0.14	-0.29	CCHOH	66.7	45	0.32	-0.51
CH_3CH_2	16.7	40	0.04	-0.53	CHCOH	66.7	50	0.77	0.15
$CHCH_2OH$	33.3	20	0.31	-0.78	CCH_2O	66.7	60	0.93	0.05
CH_2CHOH	33.3	25	0.28	-0.57	CHCHO	66.7	65	1.08	-0.38
CH_3COH	33.3	30	0.22	-0.58	CH_2CO	66.7	70	1.28	0.5
CH_2CH_2O	33.3	40	0.1	-0.7	CHCH	66.7	75	0.63	-0.09
CH_3CHO	33.3	45	0.07	-1.1	CH_2C	66.7	80	0.07	-0.64
CH_2CH_2	33.3	50	0.2	-1.03	CCOH	83.3	60	1.03	-0.29
CH_3CH	33.3	55	0.24	-0.93	CCHO	83.3	75	0.46	-0.6
CCH_2OH	50	30	0.39	-0.3	CHCO	83.3	80	0.62	-0.32
CHCHOH	50	35	0.57	-0.88	CHC	83.3	90	1.04	0.57
CH_2COH	50	40	0.57	-0.28					

From the DFT results summarized in Figure 5 and Table 2, the minimum energy pathways (MEPs) for ethane dehydrogenation are Pathway 1: CH_3CH_3 → CH_3CH_2 → CH_2CH_2 → CH_2CH → **CH_2CH** → CHC → CC and alternatively Pathway 2: CH_3CH_3 → CH_3CH_2 → CH_2CH_2 → CH_2CH → **CHCH** → CHC → CC depicted by the blue and green color code in Figure 5, respectively. Due to the higher barrier to go from CH_3C to CH_2C, that pathway is considered not feasible. Some reactions occur in parallel and are seen to have E_a difference of less than 0.05eV as in the case of reactions **2** and **3**. Although reaction **3** is slightly higher in activation energy, it is selected as the MEP due to the impossibility of generating surface poisoning specie CH_3C. No other reactions are considered to take place aside the elementary reactions. The aim of this section is to directly compare the different reactions and determine if non-feasible pathway elementary reactions need to be accounted for in future kinetic studies of the system. Below are the hypersurfaces constructed accounting for all 12 dehydrogenations using the following variables: DoDH, DoBC. Analogous to potential energy surface visualization in dynamics studies, Figure 9 gives a visual representation of the activation energy surface (AES) and reaction energy surface (RES). To generate the AES and RES figures, the smallest E_a value is representative of all data points that share the same DoDH and DoBC. All data points were generated from DFT calculations. We note that each point corresponds to a transition state in the AES and RES. This differentiates it from a potential energy surface where only saddle points are transition states.

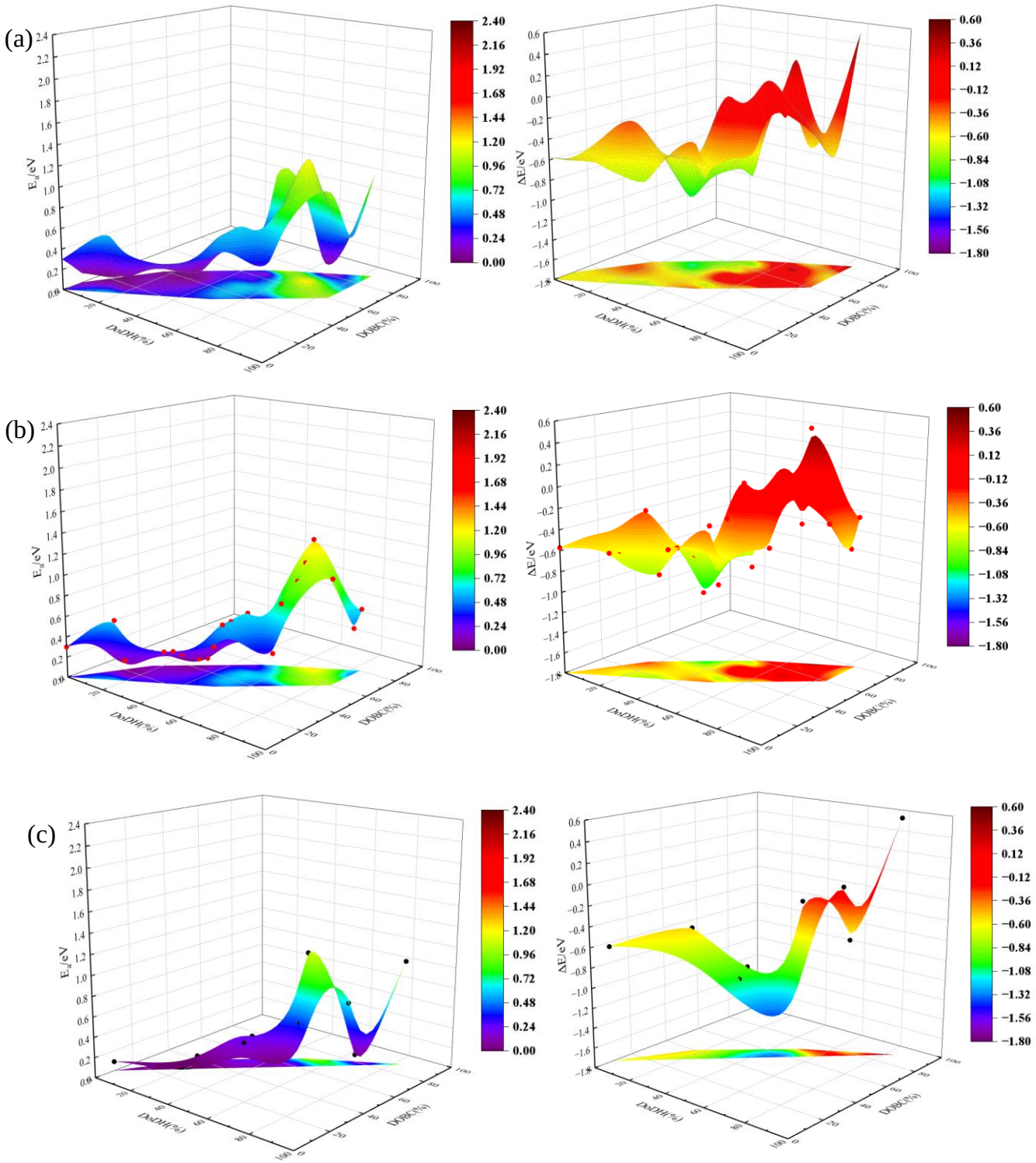

FIG. 9. Activation energy surface (left) and reaction energy surface (right) as a function of DoDH and DoBC for (a) both C_2H_x and C_2H_xO species (b) C_2H_xO species only (c) C_2H_x species only.

4. CONCLUSIONS

In this work, we employed DFT calculations to provide for the first time insights into the activation of C-H bond in ethane on Ir(100) catalyst. In other to contribute to the understanding of steam reforming of ethane. We determined the structures of the species involved in each dehydrogenation step and reported the transition states. The DFT results show that the C-H bond can be activated with relatively low activation energy in the following ranges 0.01-0.10eV, 0.20-0.50eV, 0.60-1.08eV. The Activation energy barrier changes complexly and the presence of oxygen was seen to increase the activation energy greatly. We found that CH_3C adsorbed on the surface required the most energy to activate the C-H bond, and this energy was like the activation energy of the final dehydrogenation step. Correlation between DoDH and changes in Ea or ΔE was also established as reactions with DoDH <50% has E_a well less than 1.00eV and while ΔE is most exothermic at DoDH around 50%. Showing a general increase in exothermic nature as DoDH increases from 0 to 50% and the reactions become more endothermic in nature as DoDH increases from 50%. This will lay the foundation for other works to be done on Ir(100), and the results will provide benchmark for future studies.

■ ACKNOWLEDGMENTS

RW acknowledges the support through the Gower Fellowship and the Doctoral Research Award at SIUC.

■ REFERENCES

1. Chen, G.; Liang, T.; Yoo, P.; Fadaeerayeni, S.; Sarnello, E.; Li, T.; Liao, P.; Xiang, Y., Catalytic Light Alkanes Conversion through Anaerobic Ammodehydrogenation. *ACS Catal.* **2021**, *11*, 7987-7995.
2. Wang, X.; Xu, Y., Recent Advances in Catalytic Conversion of C_5/C_6 Alkanes to Olefins: A Review. *Catal. Surv. Asia* **2022**, *26*, 245-260.

3. Arutyunov, V., Technological Prospects of Noncatalytic Partial Oxidation of Light Alkanes. *Rev. Chem. Eng.* **2021**, *37*, 99-123.
4. McDermott, W. P.; Cendejas, M. C.; Hermans, I., Recent Advances in the Understanding of Boron-Containing Catalysts for the Selective Oxidation of Alkanes to Olefins. *Top. Catal.* **2020**, *63*, 1700-1707.
5. Li, Y. M.; Fu, S. T.; Zhang, Q. Y.; Liu, H. Y.; Wang, Y. J., Recent Progress of Ga-Based Catalysts for Catalytic Conversion of Light Alkanes. *Catalysts* **2022**, *12*, 1371.
6. Qureshi, Z. S.; Arudra, P.; Bari Siddiqui, M. A.; Aitani, A. M.; Tanimu, G.; Alasiri, H., Enhanced Light Olefins Production Via N-Pentane Cracking Using Modified Mfi Catalysts. *Heliyon* **2022**, *8*, e09181.
7. Li, C.; Wang, G., Dehydrogenation of Light Alkanes to Mono-Olefins. *Chem. Soc. Rev.* **2021**, *50*, 4359-4381.
8. Kolesnichenko, N. V.; Ezhova, N. N.; Snatenkova, Y. M., Lower Olefins from Methane: Recent Advances. *Russ. Chem. Rev.* **2020**, *89*, 191-224.
9. Tian, J.; Tan, J.; Xu, M.; Zhang, Z.; Wan, S.; Wang, S.; Lin, J.; Wang, Y., Propane Oxidative Dehydrogenation over Highly Selective Hexagonal Boron Nitride Catalysts: The Role of Oxidative Coupling of Methyl. *Sci. Adv.* **2019**, *5*, eaav8063.
10. Zhu, C.; Hou, S.; Hu, X.; Lu, J.; Chen, F.; Xie, K., Electrochemical Conversion of Methane to Ethylene in a Solid Oxide Electrolyzer. *Nat. Commun.* **2019**, *10*, 1173.
11. Zhu, D.; Wang, Z.; Meng, F.; Zhao, B.; Kanitkar, S.; Tang, Y., Catalytic Conversion of Chloromethane to Olefins and Aromatics over Zeolite Catalysts. *Catal. Lett.* **2020**, *151*, 1038-1048.
12. Cordon, M. J.; Zhang, J.; Samad, N. R.; Harris, J. W.; Unocic, K. A.; Li, M.; Liu, D.; Li, Z., Ethanol Conversion to C_{4+} Olefins over Bimetallic Copper- and Lanthanum-Containing Beta Zeolite Catalysts. *ACS Sustain. Chem. Eng.* **2022**, *10*, 5702-5707.
13. Wang, S.; Jiang, Z.; Yang, J.; Tang, Y.; Liu, B., Design and Research on Preparation of C_4 Olefins by Ethanol Coupling Based on Logistic. *Energy Rep.* **2022**, *8*, 370-376.
14. Yang, M.; Fan, D.; Wei, Y.; Tian, P.; Liu, Z., Recent Progress in Methanol-to-Olefins (Mto) Catalysts. *Adv. Mater.* **2019**, *31*, e1902181.
15. Zhang, S. H.; Wang, C. M.; Zhou, X. G.; Zhu, Y. A., Elucidating the Methanol Conversion in H-Sapo-5 from First Principles: Nature of Hydrocarbon Pool and Scission Style. *Mol. Catal.* **2020**, *490*, 110948.
16. Golubev, K. B.; Batova, T. I.; Kolesnichenko, N. V.; Maximov, A. L., Synthesis of C_2–C_4 Olefins from Methanol as a Product of Methane Partial Oxidation over Zeolite Catalyst. *Catal. Commun.* **2019**, *129*, 105744.
17. Yang, S.; Zhang, L.; Wang, Z., Advances in the Preparation of Light Alkene from Carbon Dioxide by Hydrogenation. *Fuel* **2022**, *324*, 124503.
18. Wang, S.; Zhang, L.; Wang, P.; Jiao, W.; Qin, Z.; Dong, M.; Wang, J.; Olsbye, U.; Fan, W., Highly Selective Hydrogenation of Co_2 to Propane over $Gazro_x$/H-Ssz-13 Composite. *Nat. Catal.* **2022**, *5*, 1038-1050.
19. Chen, H.; Ma, N.; Wang, C.; Liu, C.; Shen, J.; Wang, Y.; Xu, G.; Yang, Q.; Feng, X., Insight into the Activation of Co_2 and H_2 on K_2o-Adsorbed Fe_5c_2(110) for Olefins Production: A Density Functional Theory Study. *Mol. Catal.* **2022**, *524*, 112323.
20. Wang, Y.; Gao, W.; Kazumi, S.; Li, H.; Yang, G.; Tsubaki, N., Direct and Oriented Conversion of Co_2 into Value-Added Aromatics. *Chem. Eur. J.* **2019**, *25*, 5149-5153.

21. Liu, M.; Yi, Y.; Wang, L.; Guo, H.; Bogaerts, A., Hydrogenation of Carbon Dioxide to Value-Added Chemicals by Heterogeneous Catalysis and Plasma Catalysis. *Catalysts* **2019**, *9*, 275.
22. Ra, E. C.; Kim, K. Y.; Kim, E. H.; Lee, H.; An, K.; Lee, J. S., Recycling Carbon Dioxide through Catalytic Hydrogenation: Recent Key Developments and Perspectives. *ACS Catal.* **2020**, *10*, 11318-11345.
23. Pawelec, B.; Guil-Lopez, R.; Mota, N.; Fierro, J. L. G.; Navarro Yerga, R. M., Catalysts for the Conversion of Co_2 to Low Molecular Weight Olefins-a Review. *Materials (Basel)* **2021**, *14*, 6952.
24. Nisa, K. S.; Suendo, V.; Sophiana, I. C.; Susanto, H.; Kusumaatmaja, A.; Nishiyama, N.; Budhi, Y. W., Effect of Base Promoter on Activity of Mcm-41-Supported Nickel Catalyst for Hydrogen Production Via Dry Reforming of Methane. *Int. J. Hydrogen Energy* **2022**, *47*, 23201-23212.
25. Akri, M., et al., Atomically Dispersed Nickel as Coke-Resistant Active Sites for Methane Dry Reforming. *Nat. Commun.* **2019**, *10*, 5181.
26. Cao, P.; Adegbite, S.; Zhao, H.; Lester, E.; Wu, T., Tuning Dry Reforming of Methane for F-T Syntheses: A Thermodynamic Approach. *Appl. Energy* **2018**, *227*, 190-197.
27. Sheshko, T. F.; Kryuchkova, T. A.; Serov, Y. M.; Chislova, I. V.; Zvereva, I. A., New Mixed Perovskite-Type Gd_{2-X} Sr_{1+X} Fe_2o_7 Catalysts for Dry Reforming of Methane, and Production of Light Olefins. *Catal. Ind.* **2017**, *9*, 162-169.
28. He, C.; Wu, S.; Wang, L.; Zhang, J., Recent Advances in Photo-Enhanced Dry Reforming of Methane: A Review. *J. Photochem. Photobiol., C* **2022**, *51*, 100468.
29. Artsiusheuski, M. A.; Verel, R.; van Bokhoven, J. A.; Sushkevich, V. L., Methane Transformation over Copper-Exchanged Zeolites: From Partial Oxidation to C–C Coupling and Formation of Hydrocarbons. *ACS Catal.* **2021**, *11*, 12543-12556.
30. dos Santos Lima, D.; Perez-Lopez, O. W., Light Olefins by Methane Partial Oxidation Using Hydrated Waste Eggshell as Catalyst. *Fuel* **2021**, *300*, 120947.
31. Han, S.; Martenak, D. J.; Palermo, R. E.; Pearson, J. A.; Walsh, D. E., Direct Partial Oxidation of Methane over Zsm-5 Catalyst: Metals Effects on Higher Hydrocarbon Formation. *J. Catal.* **1994**, *148*, 134-137.
32. Meng, S.; Li, W.; Xu, H.; Li, Z.; Li, Y.; Jarvis, J.; Song, H., Non-Thermal Plasma Assisted Catalytic Reforming of Naphtha and Its Model Compounds with Methane at near Ambient Conditions. *Appl. Catal. B: Environ.* **2021**, *297*, 120459.
33. Qureshi, Z. S.; Ellouh, M.; Aitani, A.; Akhtar, M. N.; Jin, Y.; Koseoglu, O.; Alasiri, H., Efficient Conversion of Light Paraffinic Naphtha to Aromatics over Metal-Modified Mo/Mfi Catalysts. *J. Porous Mater.* **2022**, *29*, 683-692.
34. Jarvis, J.; Wong, A.; He, P.; Li, Q.; Song, H., Catalytic Aromatization of Naphtha under Methane Environment: Effect of Surface Acidity and Metal Modification of Hzsm-5. *Fuel* **2018**, *223*, 211-221.
35. Xiong, H.; Lin, S.; Goetze, J.; Pletcher, P.; Guo, H.; Kovarik, L.; Artyushkova, K.; Weckhuysen, B. M.; Datye, A. K., Thermally Stable and Regenerable Platinum-Tin Clusters for Propane Dehydrogenation Prepared by Atom Trapping on Ceria. *Angew. Chem. Int. Ed.* **2017**, *56*, 8986-8991.
36. Searles, K.; Chan, K. W.; Mendes Burak, J. A.; Zemlyanov, D.; Safonova, O.; Coperet, C., Highly Productive Propane Dehydrogenation Catalyst Using Silica-Supported Ga-Pt Nanoparticles Generated from Single-Sites. *J. Am. Chem. Soc.* **2018**, *140*, 11674-11679.

37. Narbeshuber, T. F.; Brait, A.; Seshan, K.; Lercher, J. A., Dehydrogenation of Light Alkanes over Zeolites. *J. Catal.* **1997**, *172*, 127-136.
38. Shi, L.; Wang, Y.; Yan, B.; Song, W.; Shao, D.; Lu, A. H., Progress in Selective Oxidative Dehydrogenation of Light Alkanes to Olefins Promoted by Boron Nitride Catalysts. *Chem. Commun. (Camb)* **2018**, *54*, 10936-10946.
39. Dai, Y.; Gao, X.; Wang, Q.; Wan, X.; Zhou, C.; Yang, Y., Recent Progress in Heterogeneous Metal and Metal Oxide Catalysts for Direct Dehydrogenation of Ethane and Propane. *Chem. Soc. Rev.* **2021**, *50*, 5590-5630.
40. Chowdhury, A. D.; Weding, N.; Julis, J.; Franke, R.; Jackstell, R.; Beller, M., Towards a Practical Development of Light-Driven Acceptorless Alkane Dehydrogenation. *Angew. Chem. Int. Ed.* **2014**, *53*, 6477-81.
41. Hansen, M. H.; Nørskov, J. K.; Bligaard, T., First Principles Micro-Kinetic Model of Catalytic Non-Oxidative Dehydrogenation of Ethane over Close-Packed Metallic Facets. *J. Catal.* **2019**, *374*, 161-170.
42. Wang, G.; Zhu, X.; Li, C., Recent Progress in Commercial and Novel Catalysts for Catalytic Dehydrogenation of Light Alkanes. *Chem. Rec.* **2020**, *20*, 604-616.
43. Liu, S.; Zhang, B.; Liu, G., Metal-Based Catalysts for the Non-Oxidative Dehydrogenation of Light Alkanes to Light Olefins. *React. Chem. Eng.* **2021**, *6*, 9-26.
44. Niu, K.; Qi, Z.; Li, Y.; Lin, H.; Chi, L., Theoretical Investigation of on-Purpose Propane Dehydrogenation over the Two-Dimensional Ru–Pc Framework. *J. Phys. Chem. C* **2019**, *123*, 4969-4976.
45. Wu, C.; Wang, L.; Xiao, Z.; Li, G.; Wang, L., Effects of Van Der Waals Interactions on the Dehydrogenation of N-Butane on a Ni(111) Surface. *Chem. Phys. Lett.* **2020**, *746*, 137229.
46. Wu, C.; Wang, L.; Xiao, Z.; Li, G.; Wang, L., Understanding Deep Dehydrogenation and Cracking of N-Butane on Ni(111) by a Dft Study. *Phys. Chem. Chem. Phys.* **2020**, *22*, 724-733.
47. Grant, J. T.; Carrero, C. A.; Goeltl, F.; Venegas, J.; Mueller, P.; Burt, S. P.; Specht, S. E.; McDermott, W. P.; Chieregato, A.; Hermans, I., Selective Oxidative Dehydrogenation of Propane to Propene Using Boron Nitride Catalysts. *Science* **2016**, *354*, 1570-1573.
48. Gärtner, C. A.; van Veen, A. C.; Lercher, J. A., Oxidative Dehydrogenation of Ethane: Common Principles and Mechanistic Aspects. *ChemCatChem* **2013**, *5*, 3196-3217.
49. Liu, Y. M.; Cao, Y.; Zhu, K. K.; Yan, S. R.; Dai, W. L.; He, H. Y.; Fan, K. N., Highly Efficient Vox/Sba-15 Mesoporous Catalysts for Oxidative Dehydrogenation of Propane. *Chem. Commun. (Camb)* **2002**, 2832-3.
50. Venegas, J. M.; McDermott, W. P.; Hermans, I., Serendipity in Catalysis Research: Boron-Based Materials for Alkane Oxidative Dehydrogenation. *Acc. Chem. Res.* **2018**, *51*, 2556-2564.
51. Yan, B.; Li, W.-C.; Lu, A.-H., Metal-Free Silicon Boride Catalyst for Oxidative Dehydrogenation of Light Alkanes to Olefins with High Selectivity and Stability. *J. Catal.* **2019**, *369*, 296-301.
52. Sheng, J.; Yan, B.; Lu, W. D.; Qiu, B.; Gao, X. Q.; Wang, D.; Lu, A. H., Oxidative Dehydrogenation of Light Alkanes to Olefins on Metal-Free Catalysts. *Chem. Soc. Rev.* **2021**, *50*, 1438-1468.
53. Silberova, B.; Fathi, M.; Holmen, A., Oxidative Dehydrogenation of Ethane and Propane at Short Contact Time. *Appl. Catal. A: Gen.* **2004**, *276*, 17-28.

54. Gaab, S.; Machli, M.; Find, J.; Grasselli, R. K.; Lercher, J. A., Oxidative Dehydrogenation of Ethane over Novel Li/Dy/Mg Mixed Oxides: Structure-Activity Study. *Top. Catal.* **2003**, *23*, 151-158.
55. Nawaz, Z.; Wei, F., Light-Alkane Oxidative Dehydrogenation to Light Olefins over Platinum-Based Sapo-34 Zeolite-Supported Catalyst. *Ind. Eng. Chem. Res.* **2012**, *52*, 346-352.
56. Maiti, A.; Govind, N.; Kung, P.; King-Smith, D.; Miller, J. E.; Zhang, C.; Whitwell, G., Effect of Surface Phosphorus on the Oxidative Dehydrogenation of Ethane: A First-Principles Investigation. *J. Chem. Phys.* **2002**, *117*, 8080-8088.
57. He, Y.; Yang, Z.; Liu, Z.; Wang, P.; Guo, M.; Ran, J., Research on the Selectivity and Activity of Ethane Oxidation Dehydrogenation with Co_2 on Cr-Based Catalyst. *Chemistryselect* **2020**, *5*, 2232-2239.
58. Liang, Y.; Liu, M.; Wang, T.; Mao, J.; Wang, L.; Liu, D.; Wang, T.; Hu, W., Uv-Curing-Enhanced Organic Long-Persistent Luminescence Materials. *Adv. Mater.* **2023**, 2304820.
59. Han, J., et al., Small-Molecule-Doped Organic Crystals with Long-Persistent Luminescence. *Adv. Funct. Mater.* **2019**, *29*, 1902503.
60. Sun, H.; Liu, D.; Wang, T.; Lu, T.; Li, W.; Ren, S.; Hu, W.; Wang, L.; Zhou, X., Enhanced Internal Quantum Efficiency in Dye-Sensitized Solar Cells: Effect of Long-Lived Charge-Separated State of Sensitizers. *ACS Appl. Mater. Interfaces* **2017**, *9*, 9880-9891.
61. McCarroll, M. E.; Shi, Y.; Harris, S.; Puli, S.; Kimaru, I.; Xu, R.; Wang, L.; Dyer, D. J., Computational Prediction and Experimental Evaluation of a Photoinduced Electron-Transfer Sensor. *J. Phys. Chem. B* **2006**, *110*, 22991.
62. Zhou, X.; Liu, D.; Wang, T.; Hu, X.; Guo, J.; Weerasinghe, K. C.; Wang, L.; Li, W., Synthesis and Photophysical Studies of Triazine-Linked Porphyrin-Perylene Bismide Dyad with Long-Lived Perylene Triplet State. *J. Photochem. Photobiol. A: Chem.* **2014**, *274*, 57-63.
63. Xu, F.; Testoff, T. T.; Wang, L.; Zhou, X., Cause, Regulation and Utilization of Dye Aggregation in Dye-Sensitized Solar Cells. *Molecules* **2020**, *25*, 4478.
64. Wang, T., et al., Enhancing Photoinduced Charge Separation through Donor Moiety in Donor-Accepter Organic Semiconductors". *J. Phys. Chem. C* **2016**, *120*, 25263-25275.
65. Wang, T.; Weerasinghe, K. C.; Sun, H.; Hu, X.; Lu, T.; Liu, D.; Hu, W.; Li, W.; Zhou, X.; Wang, L., Effect of Triplet State on the Lifetime of Charge Separation in Ambipolar D-A_1-A_2 Organic Semiconductors. *J. Phys. Chem. C* **2016**, *120*, 11338-11349.
66. Wang, T.; Weerasinghe, K. C.; Ubaldo, P. C.; Liu, D.; Li, W.; Zhou, X.; Wang, L., Tuning Electron–Hole Distance of the Excitons in Organic Moleculesusing Functional Groups. *Chem. Phys. Lett.* **2015**, *618*, 142-146.
67. Walkup, L. L.; Weerasinghe, K. C.; Tao, M.; Zhou, X.; Zhang, M.; Liu, D.; Wang, L., Importance of Dynamics in Electron Excitation and Transfer of Organic Dyes. *J. Phys. Chem. C* **2010**, *114*, 19521-19528.
68. Ge, X.; Zhu, M.; Shen, J., Catalytic Performance of Silica-Supported Chromium Oxide Catalysts in Ethane Dehydrogenation with Carbon Dioxide. *React. Kinet. Catal. Lett.* **2002**, *77*, 103-108.
69. Li, X.; Liu, S.; Chen, H.; Luo, S. Z.; Jing, F.; Chu, W., Improved Catalytic Performance of Ethane Dehydrogenation in the Presence of Co_2 over Zr-Promoted Cr/Sio_2. *ACS Omega* **2019**, *4*, 22562-22573.

70. Li, X.; Zhou, Y.; Qiao, B.; Pan, X.; Wang, C.; Cao, L.; Li, L.; Lin, J.; Wang, X., Enhanced Stability of Pt/Al_2o_3 Modified by Zn Promoter for Catalytic Dehydrogenation of Ethane. *J. Energy Chem.* **2020**, *51*, 14-20.
71. Nam, J.; Celik, F. E., Effect of Tin in the Bulk of Platinum–Tin Alloys for Ethane Dehydrogenation. *Top. Catal.* **2020**, *63*, 700-713.
72. Yu, K., et al., High-Temperature Pretreatment Effect on Co/Sio_2 Active Sites and Ethane Dehydrogenation. *ACS Catal.* **2022**, *12*, 11749-11760.
73. Wang, S.; Murata, K.; Hayakawa, T.; Hamakawa, S.; Suzuki, K., Dehydrogenation of Ethane with Carbon Dioxide over Supported Chromium Oxide Catalysts. *Appl. Catal. A: Gen.* **2000**, *196*, 1-8.
74. Nakagawa, K.; Kajita, C.; Okumura, K.; Ikenaga, N.-o.; Nishitani-Gamo, M.; Ando, T.; Kobayashi, T.; Suzuki, T., Role of Carbon Dioxide in the Dehydrogenation of Ethane over Gallium-Loaded Catalysts. *J. Catal.* **2001**, *203*, 87-93.
75. Koirala, R.; Safonova, O. V.; Pratsinis, S. E.; Baiker, A., Effect of Cobalt Loading on Structure and Catalytic Behavior of Coo_x /Sio_2 in Co_2 -Assisted Dehydrogenation of Ethane. *Appl. Catal. A: Gen.* **2018**, *552*, 77-85.
76. Skubic, L.; Sovdat, J.; Teran, N.; Huš, M.; Kopač, D.; Likozar, B., Ab Initio Multiscale Process Modeling of Ethane, Propane and Butane Dehydrogenation Reactions: A Review. *Catalysts* **2020**, *10*, 1405.
77. Wu, Z.; Wegener, E. C.; Tseng, H.-T.; Gallagher, J. R.; Harris, J. W.; Diaz, R. E.; Ren, Y.; Ribeiro, F. H.; Miller, J. T., Pd–in Intermetallic Alloy Nanoparticles: Highly Selective Ethane Dehydrogenation Catalysts. *Catal. Sci. Technol.* **2016**, *6*, 6965-6976.
78. Wu, J.; Mallikarjun Sharada, S.; Ho, C.; Hauser, A. W.; Head-Gordon, M.; Bell, A. T., Ethane and Propane Dehydrogenation over Ptir/Mg(Al)O. *Appl. Catal. A: Gen.* **2015**, *506*, 25-32.
79. Vincent, R. S.; Lindstedt, R. P.; Malik, N. A.; Reid, I. A. B.; Messenger, B. E., The Chemistry of Ethane Dehydrogenation over a Supported Platinum Catalyst. *J. Catal.* **2008**, *260*, 37-64.
80. Galvita, V.; Siddiqi, G.; Sun, P. P.; Bell, A. T., Ethane Dehydrogenation on Pt/Mg(Al)O and Ptsn/Mg(Al)O Catalysts. *J. Catal.* **2010**, *271*, 209-219.
81. Zhang, Q.; Zhang, K.; Zhang, S.; Liu, Q.; Chen, L.; Li, X.; Wang, C.; Ma, L., Ga^{3+}-Stabilized Pt in Ptsn-Mg(Ga)(Al)O Catalyst for Promoting Ethane Dehydrogenation. *J. Catal.* **2018**, *368*, 79-88.
82. Seki, H.; Saito, H.; Toko, K.; Hosono, Y.; Higo, T.; Gil Seo, J.; Maeda, S.; Hashimoto, K.; Ogo, S.; Sekine, Y., Effect of Ba Addition to Ga-A-Al_2o_3 Catalyst on Structure and Catalytic Selectivity for Dehydrogenation of Ethane. *Appl. Catal. A: Gen.* **2019**, *581*, 23-30.
83. Zhang, Y.; Wang, B.; Fan, M.; Li, D.; Zhang, R., Ethane Dehydrogenation over the Single-Atom Alloy Catalysts: Screening out the Excellent Catalyst with the Dual Descriptors. *Fuel* **2021**, *306*, 121641.
84. Ko, J.; Schneider, W. F., Computational Screen of M_2p Metal Phosphides for Catalytic Ethane Dehydrogenation. *Catal. Sci. Technol.* **2022**, *12*, 5629-5639.
85. Ge, Y.; Jiang, H.; Kato, R.; Gummagatta, P., Size and Site Dependence of the Catalytic Activity of Iridium Clusters toward Ethane Dehydrogenation. *J. Phys. Chem. A* **2016**, *120*, 9500-9508.
86. Ge, X.; Sun, Q.; Shen, J. Y., A Study on Cr/Ceo_2 Catalysts and Their Catalytic Performance for Dehydrogenation of Ethane. *Chin. J. Inorg. Chem.* **2004**, *20*, 987-990.

87. Yang, Z.; Li, H.; Zhou, H.; Wang, L.; Wang, L.; Zhu, Q.; Xiao, J.; Meng, X.; Chen, J.; Xiao, F. S., Coking-Resistant Iron Catalyst in Ethane Dehydrogenation Achieved through Siliceous Zeolite Modulation. *J. Am. Chem. Soc.* **2020**, *142*, 16429-16436.
88. Batchu, S. P.; Wang, H.-L.; Chen, W.; Zheng, W.; Caratzoulas, S.; Lobo, R. F.; Vlachos, D. G., Ethane Dehydrogenation on Single and Dual Centers of Ga-Modified Γ-Al_2O_3. *ACS Catal.* **2021**, *11*, 1380-1391.
89. Saito, H.; Maeda, S.; Seki, H.; Manabe, S.; Miyamoto, Y.; Ogo, S.; Hashimoto, K.; Sekine, Y., Supported Ga-Oxide Catalyst for Dehydrogenation of Ethane. *J. Jpn. Pet. Inst.* **2017**, *60*, 203-210.
90. Shen, W.; Wang, Y.; Shi, X.; Shah, N.; Huggins, F.; Bollineni, S.; Seehra, M.; Huffman, G., Catalytic Nonoxidative Dehydrogenation of Ethane over Fe–Ni and Ni Catalysts Supported on Mg(Al)O to Produce Hydrogen and Easily Purified Carbon Nanotubes. *Energy Fuels* **2007**, *21*, 3520-3529.
91. Gobina, E.; Hughes, R., Ethane Dehydrogenation Using a High-Temperature Catalytic Membrane Reactor. *J. Membr. Sci.* **1994**, *90*, 11-19.
92. Gobina, E.; Hou, K.; Hughes, R., Ethane Dehydrogenation in a Catalytic Membrane Reactor Coupled with a Reactive Sweep Gas. *Chem. Eng. Sci.* **1995**, *50*, 2311-2319.
93. Virnovskaia, A.; Jørgensen, S.; Hafizovic, J.; Prytz, Ø.; Kleimenov, E.; Hävecker, M.; Bluhm, H.; Knop-Gericke, A.; Schlögl, R.; Olsbye, U., In Situ Xps Investigation of Pt(Sn)/Mg(Al)O Catalysts During Ethane Dehydrogenation Experiments. *Surf. Sci.* **2007**, *601*, 30-43.
94. Virnovskaia, A.; Rytter, E.; Olsbye, U., Kinetic and Isotopic Study of Ethane Dehydrogenation over a Semicommercial Pt,Sn/Mg(Al)O Catalyst. *Ind. Eng. Chem. Res.* **2008**, *47*, 7167-7177.
95. Duan, X.; Ye, L.; Xie, K., Boosted Dehydrogenation of Ethane over Porous Vanadium-Based Single Crystals. *Catal. Sci. Technol.* **2021**, *11*, 6573-6578.
96. Zhang, L.; Sun, J.; Jiang, S.; He, H.; Ren, G.; Zhai, D.; Tu, R.; Zhai, S.; Yu, T., Synergetic Effect between Pd^{2+} and Ir^{4+} Species Promoting Direct Ethane Dehydrogenation into Ethylene over Bimetallic Pdir/Ac Catalysts. *Catal. Sci. Technol.* **2022**, *12*, 3874-3885.
97. Muhlenkamp, J. A.; LiBretto, N. J.; Miller, J. T.; Hicks, J. C., Ethane Dehydrogenation Performance and High Temperature Stability of Silica Supported Cobalt Phosphide Nanoparticles. *Catal. Sci. Technol.* **2022**, *12*, 976-985.
98. Lu, J.; Aydin, C.; Browning, N. D.; Wang, L.; Gates, B. C., Sinter-Resistant Catalysts: Supported Iridium Nanoclusters with Intrinsically Limited Sizes. *Catal. Lett.* **2012**, *142*, 1445-1451.
99. Zhang, W.; Xiao, L.; Hirata, Y.; Pawluk, T.; Wang, L., The Simple Cubic Structure of Ir Clusters and the Element Effect on Cluster Structures. *Chem. Phys. Lett.* **2004**, *383*, 67-71.
100. Pawluk, T.; Hirata, Y.; Wang, L., Studies of Iridium Nanoparticles Using Density Functional Theory Calculations. *J. Phys. Chem. B* **2005**, *109*, 20817-20823.
101. Bian, Y.; Kim, M.; Li, T.; Asthagiri, A.; Weaver, J. F., Facile Dehydrogenation of Ethane on the IrO_2(110) Surface. *J. Am. Chem. Soc.* **2018**, *140*, 2665-2672.
102. Wang, L.; Williams, J. I.; Lin, T.; Zhong, C. J., Spontaneous Reduction of O_2 on Ptvfe Nanocatalysts. *Catal. Today* **2011**, *165*, 150-159.
103. Sun, K.; Wu, Z.; Wu, R.; Chen, Y.; Zhang, M.; Wang, L., Rate-Limiting Reaction of Dehydrogenative Dimerization of Ethanol to Ethyl Acetate and Hydrogen on Cu, Cu2, and Cu13 Clusters: Size Dependence. *ChemRxiv* **2023**, 10.26434/chemrxiv-2023-6w2qd.

104. Wang, L.; Ore, R. M.; Jayamaha, P. K.; Wu, Z.-P.; Zhong, C.-J., Density Functional Theory Based Computational Investigations on the Stability of Highly Active Trimetallic Ptpdcu Nanoalloys for Electrochemical Oxygen Reduction. *Faraday Discuss.* **2023**, *242*, 429-442.
105. Ge, Y.; Le, A.; Marquino, G. J.; Nguyen, P. Q.; Trujillo, K.; Schimelfenig, M.; Noble, A., Tools for Prescreening the Most Active Sites on Ir and Rh Clusters toward C-H Bond Cleavage of Ethane: Nbo Charges and Wiberg Bond Indexes. *ACS Omega* **2019**, *4*, 18809-18819.
106. Kresse, G.; Hafner, J., Ab Initio Molecular Dynamics for Liquid Metals. *Phys. Rev. B* **1993**, *47*, 558-561.
107. Kresse, G.; Furthmüller, J., Efficient Iterative Schemes for Ab Initio Total-Energy Calculations Using a Plane-Wave Basis Set. *Phys. Rev. B* **1996**, *54*, 11169-11186.
108. Blöchl, P. E., Projector Augmented-Wave Method. *Phys. Rev. B* **1994**, *50*, 17953-17979.
109. Kresse, G.; Joubert, D., From Ultrasoft Pseudopotentials to the Projector Augmented-Wave Method. *Phys. Rev. B* **1999**, *59*, 1758-1775.
110. Wu, R.; Wiegand, K. R.; Wang, L., Impact of the Degree of Dehydrogenation in Ethanol C-C Bond Cleavage on Ir(100). *J. Chem. Phys.* **2021**, *154*, 054705.
111. Wu, R.; Wiegand, K. R.; Ge, L.; Wang, L., Role of Oxygen Species toward the C–C Bond Cleavage in Steam Reforming of C_{2+} Alkanes: Dft Studies of Ethane on Ir(100). *J. Phys. Chem. C* **2021**, *125*, 14275-14286.
112. Wu, R.; Wang, L., Insights and Activation Energy Surface of the Dehydrogenation of $C_2 H_x O$ Species in Ethanol Oxidation Reaction on Ir(100). *ChemPhysChem* **2022**, *23*, e202200132.
113. Henkelman, G.; Uberuaga, B. P.; Jónsson, H., A Climbing Image Nudged Elastic Band Method for Finding Saddle Points and Minimum Energy Paths. *J. Chem. Phys.* **2000**, *113*, 9901-9904.
114. Bader, R. F. W., A Quantum Theory of Molecular Structure and Its Applications. *Chem. Rev.* **1991**, *91*, 893-928.
115. Chen, Y.; Vlachos, D. G., Hydrogenation of Ethylene and Dehydrogenation and Hydrogenolysis of Ethane on Pt(111) and Pt(211): A Density Functional Theory Study. *J. Phys. Chem. C* **2010**, *114*, 4973-4982.
116. Wang, Y.; Hu, P.; Yang, J.; Zhu, Y.-A.; Chen, D., C–H Bond Activation in Light Alkanes: A Theoretical Perspective. *Chem. Soc. Rev.* **2021**, *50*, 4299-4358.
117. Damte, J. Y.; Zhu, Z.-J.; Lin, P.-J.; Yeh, C.-H.; Jiang, J.-C., B, N-Co-Doped Graphene-Supported Ir and Pt Clusters for Methane Activation and C C Coupling: A Density Functional Theory Study. *J. Comput. Chem.* **2020**, *41*, 194-202.
118. Xiao, L.; Wang, L., Methane Activation on Pt and Pt_4: A Density Functional Theory Study. *J. Phys. Chem. B* **2007**, *111*, 1657-1663.
119. Wu, C.; Xiao, Z.; Wang, L.; Li, G.; Zhang, X.; Wang, L., Modulating Oxidation State of Ni/Ceo_2 Catalyst for Steam Methane Reforming: A Theoretical Prediction with Experimental Verification. *Catal. Sci. Technol.* **2021**, *11*, 1965-1973.
120. Wu, R.; Wang, L., Activity Enhancement of Ptir Catalysts for Complete Ethanol Oxidation Reaction by Tuning C−O Coupling Abilities. *J. Phys. Chem. C* **2022**, *126*, 21650-21666.
121. Wu, R.; Wang, L., Vinyl Alcohol Formation Via Catalytic B-Dehydrogenation of Ethanol on Ir(100). *Chem. Phys. Impact* **2021**, *3*, 100040.
122. Wu, R.; Wang, L., Insight into the Solvent Effects on Ethanol Oxidation on Ir(100). *Phys. Chem. Chem. Phys.* **2023**, *25*, 2190-2202.

123. Wu, R.; Wiegand, K. R.; Ge, L.; Wang, L., Role of Oxygen Species toward the C-C Bond Cleavage in Steam Reforming of C_{2+} Alkanes: Dft Studies of Ethane on Ir(100). *J. Phys. Chem. C* **2021**, *125*, 14275-14286.
124. Sun, K.; Zhang, M.; Wang, L., Effects of Catalyst Surface and Hydrogen Bond on Ethanol Dehydrogenation to Ethoxy on Cu Catalysts. *Chem. Phys. Lett.* **2013**, *585*, 89-94.
125. Wu, R.; Wang, L., Unveiling Alloying Effects on the Catalytic Activities of Cu_3pt and Cu_3pd for Nonoxidative Dehydrogenation and Esterification of Ethanol. *Comput. Mater. Sci.* **2021**, *196*, 110514.
126. Wu, R.; Sun, K.; Chen, Y.; Zhang, M.; Wang, L., Ethanol Dimerization to Ethyl Acetate and Hydrogen on the Multifaceted Copper Catalysts. *Surf. Sci.* **2021**, *703*, 121742.
127. Miao, B.; Wu, Z.-P.; Xu, H.; Zhang, M.; Chen, Y.; Wang, L., Dft Studies on the Key Competing Reaction Steps Towards Complete Ethanol Oxidation on Transition Metal Catalysts. *Comput. Mater. Sci.* **2019**, *156*, 175-186.
128. Xu, H.; Miao, B.; Zhang, M.; Chen, Y.; Wang, L., Mechanism of C–C and C–H Bond Cleavage in Ethanol Oxidation Reaction on Cu_2o(111): A Dft-D and Dft+U Study. *Phys. Chem. Chem. Phys.* **2017**, *19*, 26210-26220.
129. Wu, Z.; Zhang, M.; Jiang, H.; Zhong, C.-J.; Chen, Y.; Wang, L., Competitive C–C and C–H Bond Scission in the Ethanol Oxidation Reaction on Cu(100) and the Effect of an Alkaline Environment. *Phys. Chem. Chem. Phys.* **2017**, *19*, 15444-15453.
130. Miao, B.; Wu, Z.; Xu, H.; Zhang, M.; Chen, Y.; Wang, L., Ir Catalysts: Preventing Ch_3cooh Formation in Ethanol Oxidation. *Chem. Phys. Lett.* **2017**, *688*, 92-97.